Effect of Neodymium Content on Creep Properties of 9Cr-3Co-3W-Nd-B Steel

Hamaguchi, Tomoaki
Research and Development Laboratory, Nippon Steel Corporation

Mitsuhara, Masatoshi
Department of Advanced Materials Science and Engineering, Faculty of Engineering Sciences, Kyushu University

Kusuhara, Hideto
Interdisciplinary Graduate School of Engineering Sciences, Faculty of Engineering Sciences, Kyushu University

https://hdl.handle.net/2324/7161032

出版情報：ISIJ International. 62 (7), pp.1548-1555, 2022-07-15. 日本鉄鋼協会
バージョン：

ISIJ International, Vol. 62 (2022), No. 7, pp. 1548–1555
https://doi.org/10.2355/isijinternational.ISIJINT-2022-057

Effect of Neodymium Content on Creep Properties of 9Cr-3Co-3W-Nd-B Steel

Tomoaki HAMAGUCHI,[1)]* Masatoshi MITSUHARA[2)] and Hideto KUSUHARA[3)]

1) Research and Development Laboratory, Nippon Steel Corporation, 1-8 Fuso-Cho, Amagasaki, Hyogo, 660-0891 Japan.
2) Department of Advanced Materials Science and Engineering, Faculty of Engineering Sciences, Kyushu University, 6-1 Kasuga-kouen, Kasuga, Fukuoka, 816-8580 Japan.
3) Interdisciplinary Graduate School of Engineering Sciences, Faculty of Engineering Sciences, Kyushu University, 6-1 Kasuga-kouen, Kasuga, Fukuoka, 816-8580 Japan.

(*Received on February 15, 2022; accepted on March 18, 2022; originally published in Tetsu-to-Hagané, Vol. 108, 2022, No. 5, pp. 325–333*)

The effects of the neodymium content on the creep properties and microstructures of 9Cr-3Co-3W-Nd-B steel were investigated. Neodymium had a mild effect on the creep rupture strength at contents up to 0.056 mass%. This suggested that the effects of neodymium compounds and solid-dissolved neodymium were minimal in the microstructures and uniformly creep-deformed parts after normalizing and tempering heat treatment. On the other hand, the reduction of area after creep rupture was improved by the addition of neodymium. Creep rupture occurred at the prior austenite grain boundaries on steel without neodymium. Therefore, neodymium conclusively adhered to the segregated sulfur at the prior austenite grain boundaries to suppress the formation of creep cracks.

KEY WORDS: 9Cr-3Co-3W-Nd-B steel; neodymium; creep ductility.

1. Introduction

It is known that 9Cr ferritic heat-resistant steels, represented as ASME Gr. 91 steels, are commonly used as a material for boilers in ultra-supercritical thermal power plants; however, there is one issue in that the creep strength in the heat-affected zone of welded joints decreases.[1–4)] A decreased creep rupture ductility has also been reported for ASME Gr. 92 steels after long-term use.[5)] In recent years, a 9Cr–3Co–3W–Nd–B steel was developed as a heat-resistant steel with improved long-term creep strength and creep rupture ductility of its welded joints, which are the problems of the above-mentioned conventional 9Cr-based heat-resistant steels.[6)] The excellent long-term creep strength of 9Cr–3Co–3W–Nd–B steel welded joints is achieved by tuning the amounts of added boron and nitrogen and maintaining the amount of grain boundary precipitates after welding and heat treatment using coarser prior austenite grains compared to a conventional steel.[7)] Furthermore, the excellent creep rupture ductility is realized by fixing the sulfur that is segregated at the prior austenite grain boundaries as neodymium sulfide by adding neodymium.

Neodymium is used in various fields in the fabrication of neodymium magnets, which are rare-earth permanent magnets; however, there are few examples of its application in heat-resistant steels. Some research examples include a study that reported the precipitation of NdN and improvement in the creep strength of welded joints of a 0.1C–11Cr–3W–3Co–V–Nb–Ta–Nd–N steel, which is one of the precursors for the development of 9Cr–3Co–3W–Nd–B steel at high temperatures (over 1 200°C).[8)] As another example, Shen *et al.* confirmed neodymium carbonitrides and neodymium in intermetallic compounds in normalized and tempered materials of 11Cr-based steels with 0.03 mass% neodymium addition.[9)] There have also been reports of improving creep rupture ductility by adding neodymium to 1.25Cr steels[10)] and 304-series stainless steels.[11)]

Thus, 9Cr–3Co–3W–Nd–B steel is the first practical heat-resistant steel among the few research examples that contains neodymium. In this paper, we describe the effects of neodymium content on the mechanical properties (including creep properties) of this steel and its microstructure. ASME Code Case 2839 specifies the amount of neodymium added in this steel as 0.010–0.060 mass%, and we investigated the addition of neodymium amounts in this range.

2. Experimental Methods

In the experiments, 9Cr–3Co–3W–Nd–B steel specimens with different neodymium contents were melted

---

* Corresponding author: E-mail: hamaguchi.84x.tomoaki@jp.nipponsteel.com

in a vacuum melting furnace in the laboratory, and steel plates with thicknesses of 15 mm were manufactured by hot forging and hot rolling. An obtained steel sheet was subjected to normalizing heat treatment at 1 070–1 170°C and tempering heat treatment at 750–790°C according to ASME Code Case 2839 to prepare a test material. **Table 1** lists the chemical composition analysis results of the test materials. The aim of this study was confirmed in that we manufactured Steels B and C with neodymium contents of 0.015 mass% and 0.056 mass%, respectively; for comparison, Steel A, to which neodymium was not added, was also produced. Optical microscopy, scanning electron microscopy (SEM), and transmission electron microscopy (TEM) were conducted for observing the microstructure. The optical microscopy observations were conducted on materials corroded by a Vilella etch. The acceleration voltages during the electron microscopy observations were 25 kV and 200 kV. Crystal orientation maps were obtained using the electron backscatter diffraction (EBSD) method. TSL Solutions OIM Analysis 6 was used for the EBSD data analysis. The austenite grains prior to the martensitic transformation were also reconstructed from the EBSD data using the prior austenite reconstruction software12) developed by Hata *et al.* The amounts of the precipitates in the test materials were analyzed by electrolyzing the parent phase with a 10% acetylacetone–1% tetramethylammonium chloride–methanol solution and conducting high-frequency inductively coupled plasma emission spectroscopy on the extracted residues. The Vickers hardness at 20°C with a pressing load of 10 kgf was measured at five points, and the average value was calculated to evaluate the mechanical properties of each test material. The creep characteristics were evaluated by creep rupture tests at 110 MPa–200 MPa at 600°C and 650°C.

3. Experimental Results and Discussion

3.1. Heat-treated Material Evaluation

Figure 1 shows the optical microstructures at the center of the wall thickness of each test material and the five-point average value of each Vickers hardness measurement. All steels presented a typical lath martensite structure, and no delta ferrite was confirmed within the observation range. The Vickers hardness ranged from 237 to 241, and there was almost no effect of the neodymium content on the Vickers hardness.

Following this, the microstructure was confirmed by the SEM-EBSD method, to investigate the crystal grain size of a test material. **Figure 2** shows the crystal orientation maps obtained from the SEM-EBSD tests of the test materials and the maps reconstructed from the crystal orientation maps to austenite grains prior to the martensitic transformation by the austenite reconstruction method. The black lines denote high-angle grain boundaries with a crystal orientation angle difference of at least 15° between adjacent pixels. Specifically, the crystal orientation maps show approximate block boundaries, packet boundaries, and prior austenite grain boundaries, whereas the reconstructed maps show the approximate austenite grain boundaries. The sizes of the austenite grains are uniform within the observation ranges of all test materials, and they are the same at approximately 300 μm, regardless of the neodymium content. The conditions of normalizing heat treatment to form the prior austenite grains were the same. Therefore, neodymium had a small effect on the prior austenite grain size.

Figure 3 shows the results of the extracted residue analysis conducted to confirm the precipitates of the test materials. The total residue amount was slightly higher in Steel B than those in Steels A and C, although the amounts of the constituent elements in all residues were the same. Chromium was the most abundant element in all residues, followed by iron, tungsten, niobium + tantalum, and vanadium. A small amount of neodymium residue was also confirmed in Steels B and C, in which neodymium was added. Temperature changes of the equilibrium phase fraction of each phase were calculated using Thermo-Calc13) to discuss the type of residue. The Thermo-Calc version was 2020a, the database was FE6, the total amount of the calculated chemical composition was 1 mol, and the main elements such as iron and chromium were selected for the calcula-

Table 1. Chemical compositions (in mass%) of Steels A, B, and C.

Steels	C	Si	Mn	P	S	Cr	W	Co	Ni	V	Nb+Ta	Nd	B	Sol.Al	N	O
A	0.07	0.25	0.51	0.014	0.001	9.06	3.0	3.03	0.10	0.18	0.08	<0.001	0.010	0.003	0.011	0.0080
B	0.08	0.22	0.51	0.015	0.001	8.95	3.0	2.98	0.10	0.19	0.08	0.015	0.010	0.005	0.011	0.0050
C	0.08	0.25	0.52	0.014	0.001	9.00	3.0	2.99	0.10	0.20	0.08	0.056	0.009	0.010	0.010	<0.001

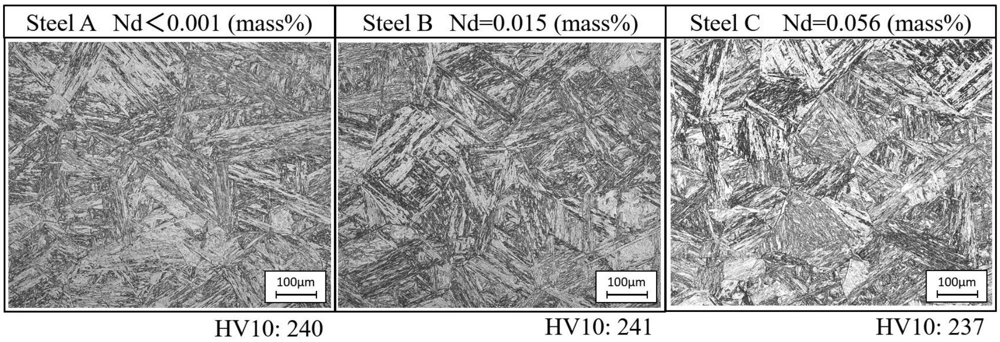

Fig. 1. Optical microstructures and Vickers hardness of tempered Steels (a) A, (b) B, and (c) C.

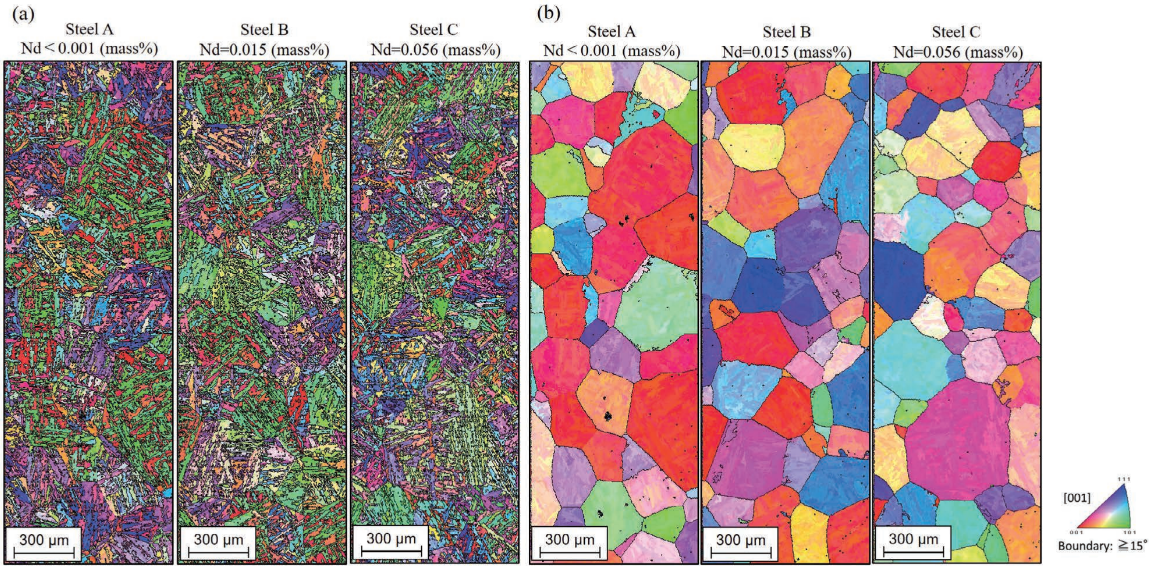

Fig. 2. Crystal orientation maps of the (a) martensite phase and (b) reconstructed prior austenite phase in tempered Steels A, B, and C.

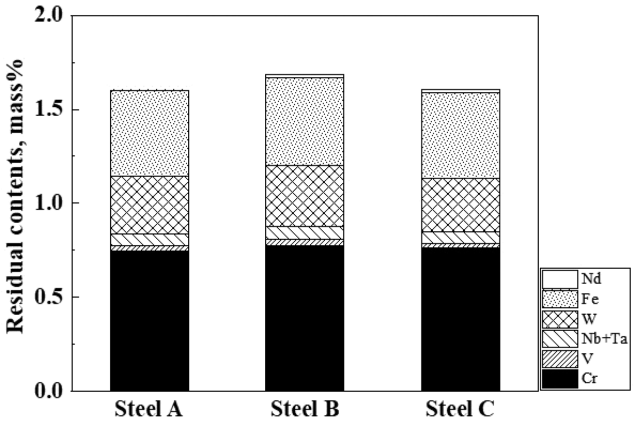

Fig. 3. Quantitative analysis of the extracted residue from tempered Steels A, B, and C.

tion. Neodymium does not have a thermodynamic database and is excluded from the calculated compositions. **Figure 4** shows the calculation results. The BCC phase is stable at 1 230–1 490°C and below 860°C, and it is estimated that delta ferrite does not form in the normalizing temperature range of 1 070–1 170°C. BN and (Nb, Ta) C are the equilibrium phases, in addition to the FCC phase of the parent phase, at the normalizing temperature. The (Nb, Ta) C, VN, BN, M_6C, $M_{23}C_6$, and Laves phases are the equilibrium phases in addition to the BCC phase of the parent phase, at the tempering temperature of 750–790°C. Therefore, it is suggested that the (Nb, Ta) C, VN, BN, M_6C, $M_{23}C_6$, and Laves phases precipitate as a result of the normalizing and tempering heat treatments, and it is considered that the detected residues in Fig. 3 are due to these precipitates.

Concurrently, with regards to the neodymium content, none was detected in Steel A, which did not contain any neodymium additions, and 0.017 mass% and 0.019 mass% of neodymium were detected in Steels B and C, respectively. Comparing the neodymium amounts listed in Table 1, the neodymium amount in the residue of Steel B is 0.002 mass% higher than that of Steel C; however, if this is considered as a measurement error, then almost all neodymium in Steel B exists as a compound. Concurrently, in Steel C, the neodymium content in the residue is 0.019 mass% compared to 0.056 mass% in Table 1, which suggests that over half of neodymium is in a solid solution. It cannot be determined from Fig. 4 whether neodymium is a constituent element of the precipitates during heat treatment; however, it may exist as oxides and sulfides at high temperatures near the melting point. The free energies for the formation of neodymium oxides and sulfides are not found in the existing literature. However, the free energy for forming oxides of cerium, which is also a rare earth element as neodymium, is the lowest value following those of calcium and beryllium at 1 380°C which is the melting point in the calculations of this steel. Moreover, the free energy of sulfide formation is the lowest among those of the elements published in the literature.[14)] Cerium is a different element from neodymium; however, assuming that their free energies are equivalent because both are rare-earth elements, there is a possibility that a neodymium compound is formed an oxide or a sulfide during the melting of the steel and is detected as a residue. Furthermore, as reported by Shen *et al.*, a residue may contain Nd carbonitride.[9)]

3.2. Creep Characteristics

The creep rupture test results of Steels A–C at 600°C and 650°C obtained in this study are shown in **Fig. 5** along with the average strength line (solid line) that is regressed with the Larson–Miller parameter using the data obtained for over 500 h for this steel and the lower limit of the 95% confidence interval (dashed line). All rupture data show a creep strength above the lower limit of the 95% confidence interval. Specifically, it can be considered that neodymium is present in Steels B and C, with Steel C also including neodymium dissolved in the parent phase; however, it can be seen that both forms of neodymium have almost no effect on the creep rupture strength. **Figure 6** displays the relationship between the creep rupture elongation and the rupture time. The creep rupture elongation showed values of 10–30% for all test materials; however, it tended to decrease as the creep time increased. Steel A, to which no neodymium was added,

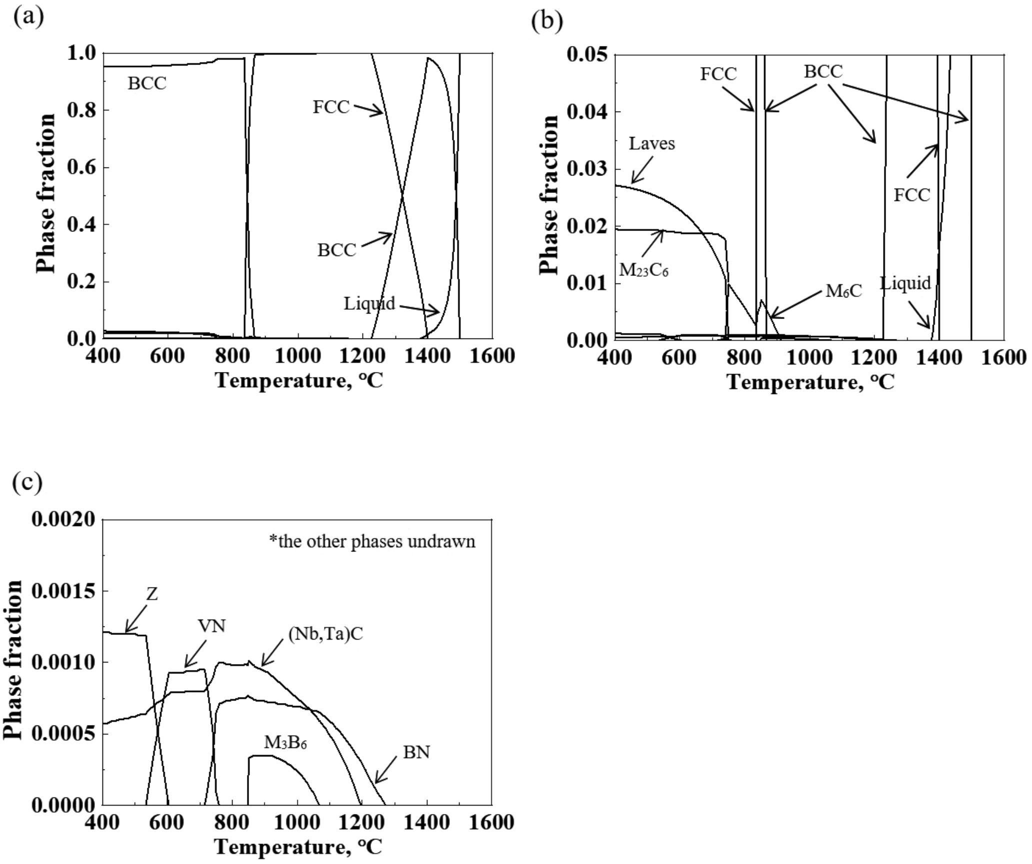

Fig. 4. Phase fractions of the Fe-9Cr-3Co-3W-B system as a function of temperature calculated by Thermo-Calc: (a) entire range of phase fraction, (b) phase fraction < 0.05, and (c) phase fraction < 0.0020.

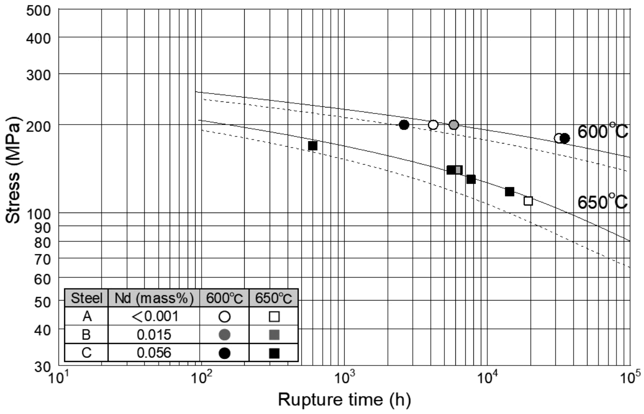

Fig. 5. Creep rupture strengths of steels A, B, and C at 600°C and 650°C. The solid and dashed lines represent the average strengths and 95% confidence limits of 9Cr-3Co-3W-Nd-B steel, respectively.

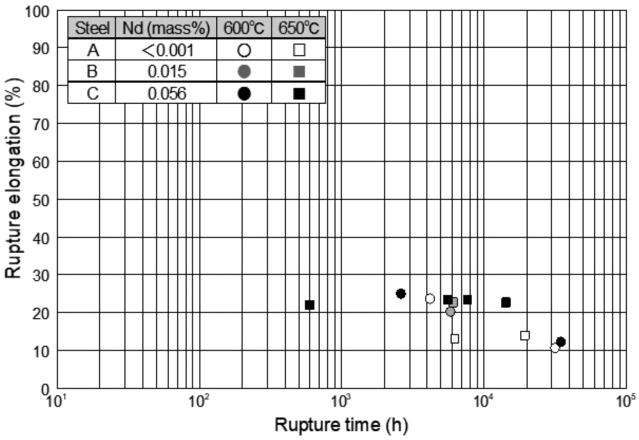

Fig. 6. Rupture elongations as a function of the rupture time in Steels A, B, and C at 600°C and 650°C.

tended to have a slightly smaller elongation at rupture than Steels B and C; however, the relationship was ambiguous. **Figure 7** presents the relationship between the reduction of area and the rupture time. Under the same conditions of 650°C and 140 MPa, the reduction of are of Steel A was approximately 33%, whereas those of Steel B (which had a neodymium addition of 0.015 mass%) and Steel C (0.056 mass% addition) were over 75%. Furthermore, Steel C showed a large reduction of area over 50% even after 30 000 h. Therefore, it can be inferred that, at least, the added neodymium has the effect of improving the rupture ductility of this steel when it is within the ASME control value range.

Figure 8 shows the creep curves of the test materials under the conditions of 650°C and 140 MPa. The rupture time was longest for Steel A, which did not include any neodymium addition, and shortest for Steel C, which had 0.056 mass% neodymium; however, their difference was small. Concurrently, the rupture elongation was 13% for Steel A and approximately 23% for Steels B and C, which included neodymium. As shown in Fig. 8(a), the reduction of area is 33% for Steel A, which does not include any neodymium addition.; concurrently, the values are high at 75% and 89% in Steels B and C, respectively, which include neodymium. Comparison of the creep rates showed that all three steels had similar creep curves, with the minimum creep rate at approximately 1 × 10^{-6}(h^{-1}). The creep rate–creep strain curve in Fig. 8(c) shows that the strain rate of Steel B increases until just prior to rupture, after which rupture occurs, whereas those of Steels A and C sharply increase from the accelerated creep region, following which rupture occurs.

3.3. Microstructures of Creep Rupture Material

As mentioned in the previous section, the neodymium content had a small effect on the creep rupture time and the minimum creep rate, whereas it had a significant effect on the creep rupture ductility. Here, we present the observations of the microstructures of the creep rupture test materials at

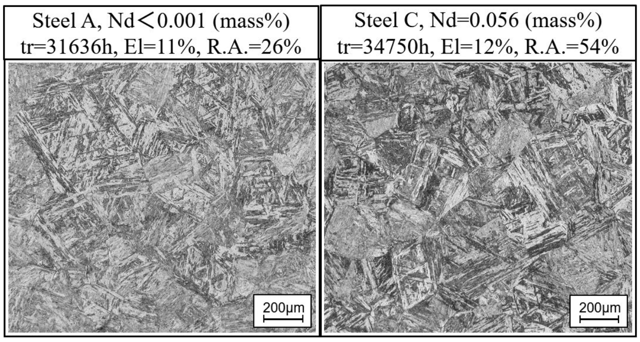

Fig. 9. Optical microstructures of the gauge portion after creep tests at 600°C under a stress of 180 MPa in Steels (a) A and (b) C. The loading direction is horizontal and the observation position is at least 10 mm away from the sample.

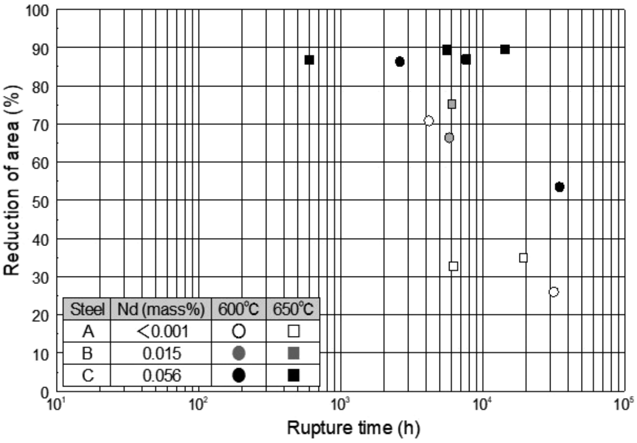

Fig. 7. Reduction of area as a function of the rupture time in Steels A, B, and C at 600°C and 650°C.

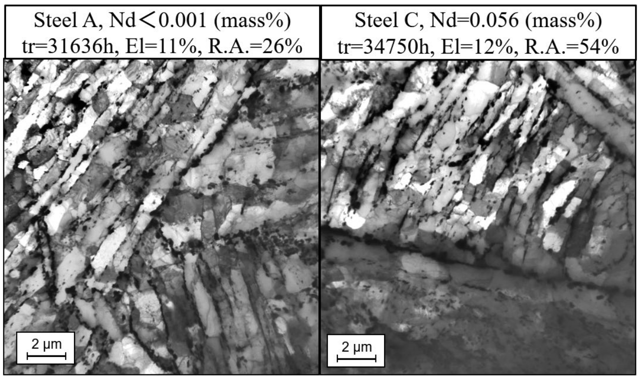

Fig. 10. TEM bright-field images of the gauge portion after creep tests at 600°C under a stress of 180 MPa in Steels (a) A and (b) C. The observation position is at least 10 mm away from the sample.

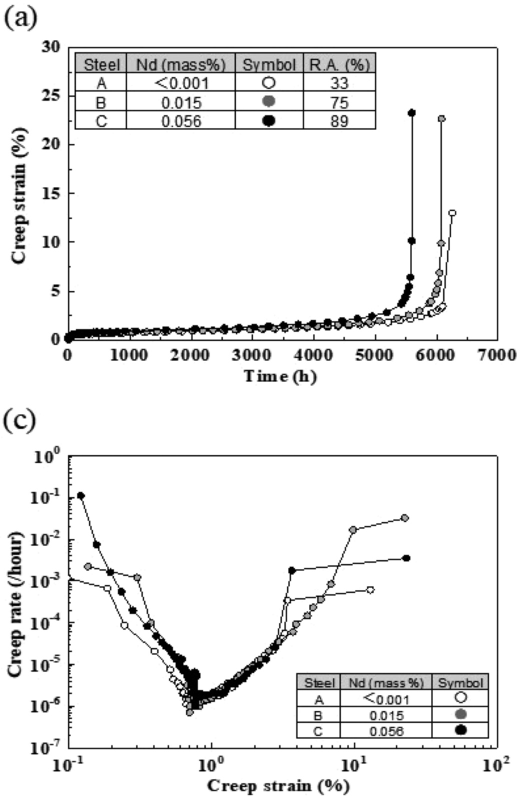

Fig. 8. Creep curves tested in Steels A, B and C at 650°C under a stress of 140 MPa: (a) time-strain curves, (b) time-creep strain rate curves, and (c) strain-creep strain rate curves.

600°C and 180 MPa of Steels A and C, which had the longest rupture time and presented differences in reduction of area. From the results, we discuss the relationship between the neodymium content and the creep characteristics.

Steel A, which did not include any neodymium addition, had a creep rupture time of 31 636 h, a creep rupture elongation of 11%, and a reduction of area of 26%. Steel C, which had a 0.056 mass% neodymium addition, had a creep rupture time of 34 750 h, a creep rupture elongation of 12%, and a reduction of area of 54%. **Figure 9** shows the optical microstructures of the gauge portion of the creep rupture test materials, and **Fig. 10** presents their TEM bright-field images. The horizontal direction in Fig. 9 is the stress-loading direction, and the observation position in both Figs. 9

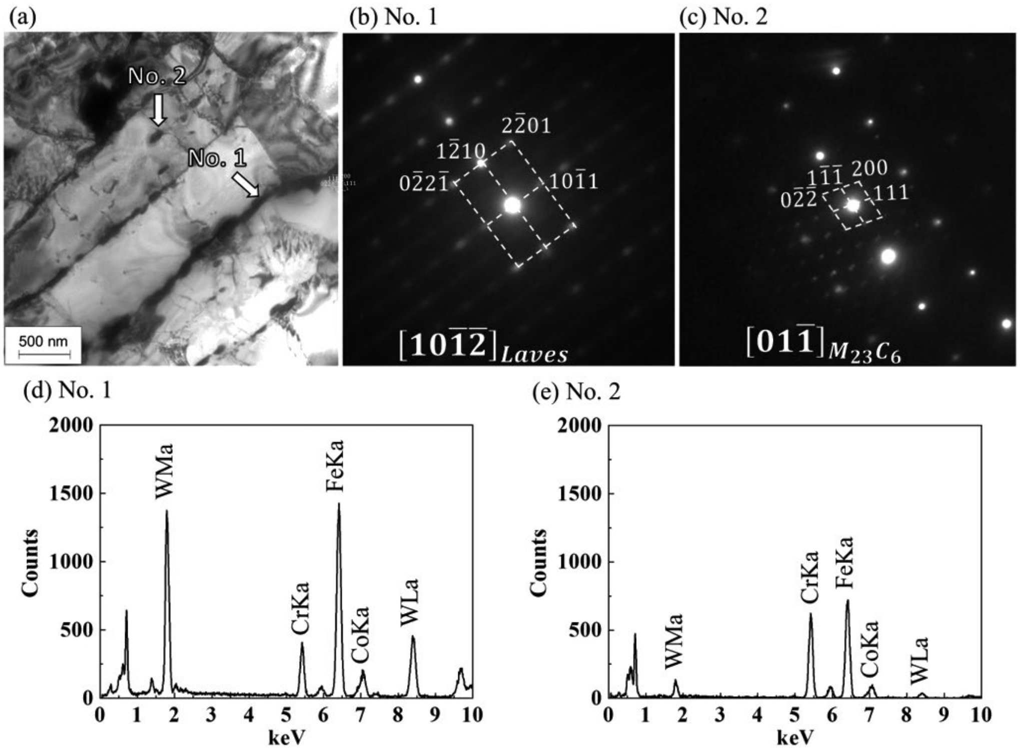

Fig. 11. (a) TEM bright-field image, (b), (c) diffraction patterns of the Laves phase and $M_{23}C_6$ carbides, and (d), (e) EDS analysis of the Laves phase and $M_{23}C_6$ carbides after creep tests at 600°C under a stress of 180 MPa in steel A.

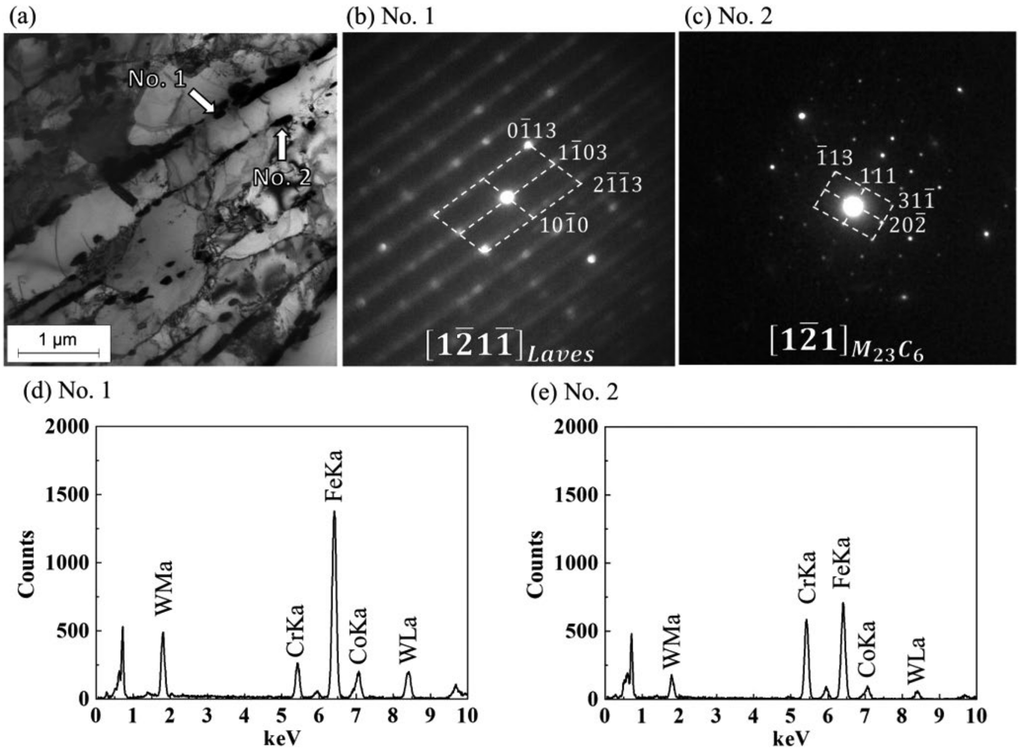

Fig. 12. (a) TEM bright-field image, (b), (c) diffraction patterns of the Laves phase and $M_{23}C_6$ carbides, and (d), (e) EDS analysis of the Laves phase and $M_{23}C_6$ carbides after creep tests at 600°C under a stress of 180 MPa in steel C.

and 10 is approximately 10 mm from the rupture part. Both Steel A and C test materials exhibited no external changes in the martensite structure in the gauge portion, even after experiencing creep deformation for over 30 000 h. Furthermore, the lath structure maintained a plate-like shape with a large aspect ratio. **Figures 11** and **12** show the electron diffraction pattern and EDS point analysis results of the precipitates of Steels A and C, respectively, from different fields of view than those of Fig. 10. The $M_{23}C_6$ and Laves phases were present at the lath boundaries in both cases, and the coverage of the lath boundary by these phases was high. $M_{23}C_6$ was also confirmed to exist in the lath regions. The above-mentioned microstructural characteristics were observed in both Steels A and C, and it can be inferred that the neodymium addition has a small effect on the coarsening and morphologies of the martensite structures and the precipitates. The Nd carbonitrides reported by Shen *et al.*[9)] were also not found in Steel C, which included a neodymium addition, within the observation range.

Concurrently, there were clear differences in reduction of area; therefore, we compared the microstructures near the rupture parts of the creep rupture test materials. **Figure 13** shows the low- and high-magnification optical microstructures in the cross-sections near the fractured parts of the creep rupture test materials of (a) Steel A and (b) Steel C. Many cracks were observed near the rupture surface of Steel A, which had a small reduction of area. Furthermore, after confirmation of the martensite structure along the main crack that caused the rupture, no elongation of the structure was observed in the load-bearing direction. Concurrently, Steel C, which contains neodymium addition, exhibited a low frequency of cracks near the rupture surface, and its martensite structure extended in the load-bearing direction. **Figure 14** shows the crystal orientation maps near the ruptured parts of Steels A and C as well as their crystal orientation maps, the latter were reconstructed from the prior austenite grains. Steel A exhibited cracks, which were presumed to have been due to the creep deformation at the prior austenite grain boundaries approximately perpendicular to the load-bearing direction, which is the horizontal direction in the figure. Furthermore, the martensite structure was maintained despite the closeness to the rupture surface, and no significant changes were observed in its shape. Concurrently, Steel C presented no cracks at the grain boundaries, showing only creep voids at the scale of a few dozen micrometers. Furthermore, the martensite structure was significantly elongated in the load-bearing direction, and the martensite structure was deformed in a ductile manner immediately before the creep rupture and area reduction of the test material. The above-mentioned microstructure observation results clarified that Steel A exhibited a rupture morphology with poor ductility compared with Steel C, in which cracks were preferentially generated at the prior austenite grain boundaries, which linked together to induce rupture. These differences in the rupture morphologies of Steels A and C, neodymium inclusions in Steel C, as shown in Fig. 3, and binding of sulfur to neodymium at the grain boundaries to form compounds and purify the grain boundaries, as reported by Nakashima[10)] and Okada[11)] suggest that the formation of neodymium inclusion reduced the sulfur that was segregated at the prior austenite grain boundaries and improved the creep rupture ductility.

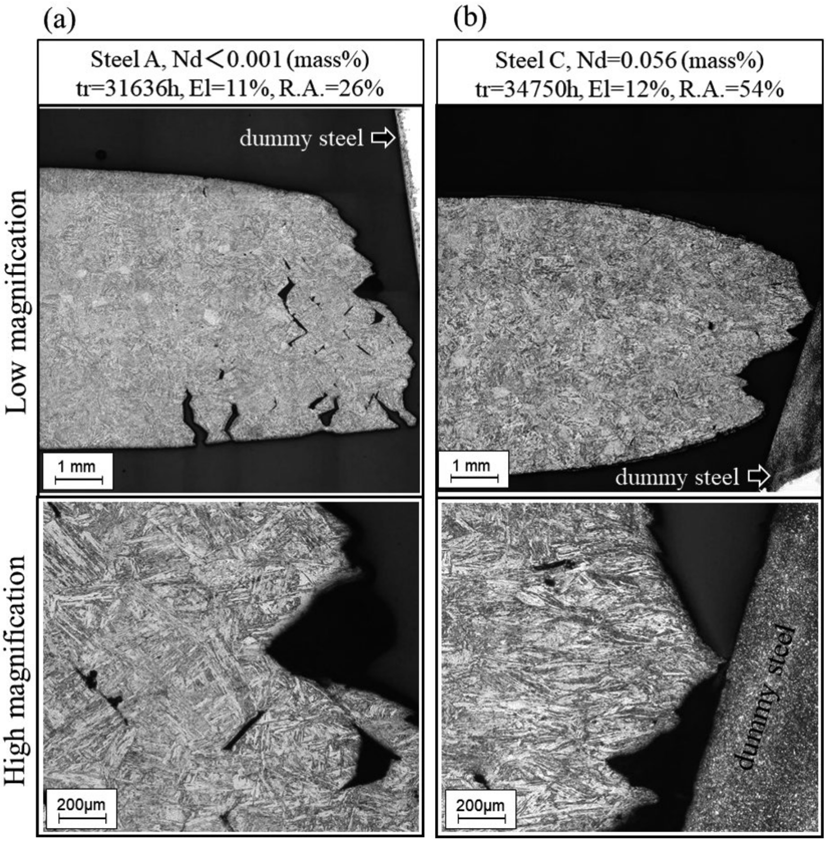

Fig. 13. Optical microstructures of the near-rupture portion after creep tests at 600°C under a stress of 180 MPa in Steels (a) A and (b) C.

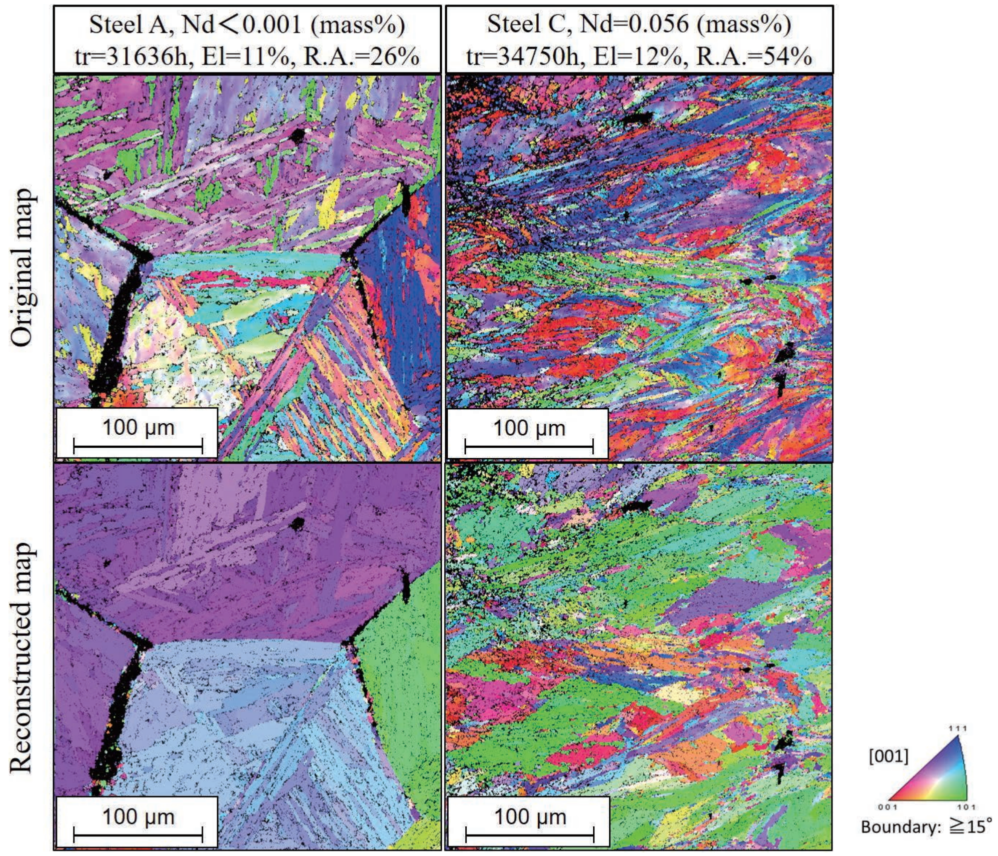

Fig. 14. Crystal orientation maps after creep tests at 600°C under a stress of 180 MPa in Steels A and C: (a), (b) original martensite phase, and (c), (d) reconstructed prior austenite phase.

4. Conclusions

We investigated the effects of neodymium content on the creep properties and microstructure of 9Cr–3Co–3W–Nd–B steels, which improved the creep strength of welded joints and creep rupture ductility of the base material. Neodymium was found to have a small effect on the creep rupture strength at contents up to 0.056 mass%. This is in good agreement with the fact that neodymium compounds and solid-dissolved neodymium have hardly any effect on the microstructure and creep deformation after normalizing and tempering heat treatments. Concurrently, neodymium contributed to the improvement in the reduction of area, regardless of the neodymium content. Steels without any neodymium addition exhibited a rupture morphology with poor ductility because of cracks preferentially forming and linking at the prior austenite grain boundaries. It could be inferred that the neodymium-induced desulfurization effect of the sulfur that was segregated at the prior austenite grain boundaries suppresses the formation of creep cracks and improves the rupture ductility.

REFERENCES

1) K. Kimura and Y. Takahashi: Proc. ASME 2012 Pressure Vessels and Piping Conf., ASME, New York, (2012), 309. https://doi.org/10.1115/PVP2012-78323
2) M. Yaguchi, T. Matsumura and K. Hoshino: Proc. ASME 2012 Pressure Vessels and Piping Conf., ASME, New York, (2012), 317. https://doi.org/10.1115/PVP2012-78393
3) K. Kimura and M. Yaguchi: Proc. ASME 2016 Pressure Vessels and Piping Conf., ASME, New York, (2016), V06BT06A014. https://doi.org/10.1115/PVP2016-63355
4) M. Yaguchi, K. Nakamura and S. Nakahashi: Proc. ASME 2016 Pressure Vessels and Piping Conf., ASME, New York, (2016), V06BT06A013. https://doi.org/10.1115/PVP2016-63316
5) F. Abe: *Mater. High Temp.*, **37** (2020), 243. https://doi.org/10.1080/09603409.2020.1771659
6) A. Iseda, M. Yoshizawa, H. Okada, T. Hamaguchi, H. Hirata, K. Joutoku, T. Ono and K. Tanaka: *Therm. Nucl. Power*, **12** (2016), 49 (in Japanese). https://doi.org/10.14942/tenpes.12.49
7) T. Hamaguchi, S. Kurihara, H. Hirata and H. Okada: *Mater. Sci. Eng. A*, **831** (2022), 142231. https://doi.org/10.1016/j.msea.2021.142231
8) M. Igarashi and Y. Sawaragi: Proc. Int. Conf. on Power Engineering 1997 (ICOPE-97), JSME, Tokyo, (1997), 107.
9) Y. Shen, X. Zhou and Z. Shang: *Met. Mater. Int.*, **22** (2016), 459. https://doi.org/10.1007/s12540-016-5696-3
10) T. Nakashima, K. Miyata, H. Hirata, M. Igarashi and A. Iseda: Advances in Materials Technology for Fossil Power Plants, ASM International, Materials Park, OH, (2008), 129.
11) H. Okada, M. Igarashi, M. Hamanaka, K. Ogawa and T. Osuki: Proc. 2nd ECCC Creep Conf., (Zurich), DEStech Publications, Inc., Lancaster, PA, (2009), 551.
12) K. Hata, K. Fujiwara, K. Kawano, M. Sugiyama, T. Fukuda and T. Kakeshita: *ISIJ Int.*, **58** (2018), 742. https://doi.org/10.2355/isijinternational.ISIJINT-2017-639
13) L. Hoglund: Foundation of Computational Thermodynamics, Royal Institute of Technology, Stockholm, (1997), 1.
14) The Japan Institute of Metals and Materials, ed.: Metal Databook, 4th ed., Maruzen, Tokyo, (2004), 91.